Low-Temperature Protein Dynamics of the B800 Molecules in the LH2 Light-Harvesting Complex: Spectral Hole Burning Study and Comparison with Single Photosynthetic Complex Spectrosco...

ARTICLE *in* THE JOURNAL OF PHYSICAL CHEMISTRY B · FEBRUARY 2010

Impact Factor: 3.3 · DOI: 10.1021/jp9089358 · Source: PubMed

Low-Temperature Protein Dynamics of the B800 Molecules in the LH2 Light-Harvesting Complex: Spectral Hole Burning Study and Comparison with Single Photosynthetic Complex Spectroscopy

Daniel Grozdanov,[†,‡] Nicoleta Herascu,[†,‡] Tõnu Reinot,[§] Ryszard Jankowiak,[||] and Valter Zazubovich*[,†]

Department of Physics, Concordia University, 7141 Sherbrooke Street West, Montreal, Quebec H4B 1R6, Canada, IPRT and Ames Laboratory, U.S. Department of Energy, Ames, Iowa 50011, Department of Chemistry, Kansas State University, Manhattan, Kansas 66506

Received: September 15, 2009; Revised Manuscript Received: February 2, 2010

Previously published and new spectral hole burning (SHB) data on the B800 band of LH2 light-harvesting antenna complex of *Rps. acidophila* are analyzed in light of recent single photosynthetic complex spectroscopy (SPCS) results (for a review, see Berlin et al. *Phys. Life Rev.* **2007**, *4*, 64.). It is demonstrated that, in general, SHB-related phenomena observed for the B800 band are in qualitative agreement with the SPCS data and the protein models involving multiwell multitier protein energy landscapes. Regarding the quantitative agreement, we argue that the single-molecule behavior associated with the fastest spectral diffusion (smallest barrier) tier of the protein energy landscape is inconsistent with the SHB data. The latter discrepancy can be attributed to SPCS probing not only the dynamics of of the protein complex per se, but also that of the surrounding amorphous host and/or of the host−protein interface. It is argued that SHB (once improved models are developed) should also be able to provide the average magnitudes and probability distributions of light-induced spectral shifts and could be used to determine whether SPCS probes a set of protein complexes that are both intact and statistically relevant. SHB results are consistent with the B800 → B850 energy-transfer models including consideration of the whole B850 density of states.

1. Introduction

Spectral hole burning (SHB) has been extensively used for more than 20 years to explore light harvesting, excitation energy transfer (EET), and primary charge-separation processes in various photosynthetic complexes.[1−3] However, those familiar with the field might ask whether this well-established technique is by now applicable only to the study of complexes from new organisms or new photosynthetic complexes or whether one could extract new information that previously was believed to be unobtainable with SHB. In particular, one could ask whether SHB could be applied for the determination of entire lifetime distributions, and not only the average lifetime (at a given wavelength) as is commonly done in SHB. The presence of such distributions is an inevitable consequence of disorder in photosynthetic complexes,[4−6] and their determination could serve as an additional type of experiment/analysis allowing for the refinement of the assignments of site excitation energies and coupling energies in various photosynthetic complexes. These assignments are still a matter of debate for practically every known photosynthetic complex.

The lifetime distribution data could be directly obtained from single photosynthetic complex spectroscopy (SPCS) experiments. However, such experiments are technically much more demanding than SHB experiments, and the collection of statistically meaningful amounts of data requires a great deal of time. Moreover, as reported in ref 7 and discussed below, light-induced spectral diffusion in SPCS experiments can affect the measured line widths. It is obvious that reliable determination of the EET (or charge separation[8,9]) rate distribution parameters using SHB requires that these parameters be disentangled from the effects due to near-equilibrium protein dynamics characterized by distributions of barrier heights and/or widths on the very complex protein energy landscapes.[10−12] This can be achieved only with detailed information on the processes responsible for the hole burning kinetics. [Here, we use "SHB kinetics" as a generalized term including not only the irradiation dose dependence of the resonant hole depth,[13−15] but also the evolution of the hole shape, including the antihole due to the nonphotochemical hole burning (NPHB) process.]

This, in turn, leads us to the question of which features of low-temperature protein dynamics are responsible for the NPHB kinetics and, in more general terms, how much the SHB kinetics in proteins differs from that in glasses and polymers. It is well-known that optically observable low-temperature dynamics of various pigments in a protein environment exhibit similarities as well as differences compared to those in glasses and polymers (see refs 16 and 17 for recent reviews). SPCS has been applied for detailed studies of spectral diffusion in the LH2 light-harvesting complex of purple bacteria.[7,10,16,18−25] It has been demonstrated that light-induced spectral diffusion behavior in this system is a reflection of the hierarchy of tiers in the protein energy landscape.[10] Spectral shifts with different magnitudes (from less than 1 cm^{-1} to a couple hundred wavenumbers) have been observed with shift probabilities that decrease with increasing magnitude of the shift.[10,19] (More details are provided in the Discussion and Simulations section.) One goal of this

* Corresponding author. E-mail: vzazubov@alcor.concordia.ca.
[†] Concordia University.
[‡] The first two authors contributed equally to the work described in this article.
[§] IPRT and Ames Laboratory.
[||] Kansas State University.

10.1021/jp9089358
Published on Web 02/18/2010

work is to determine whether SHB results, in particular, the shape of the NPHB antihole (sometimes somewhat misleadingly called a "photoproduct", despite the fact that no photochemical reactions occur in the case of NPHB), are in agreement with data obtained by SPCS[7,10,16,18−25] and with available theoretical SHB models[13−15,26]

There is also additional motivation for studying the antihole shapes (i.e., the light-induced line shift distributions) in photosynthetic complexes. Specifically, in photosynthetic complexes, the pigments are often closely spaced and strongly interacting. These interactions result in delocalization of the excited states, shifts of the spectral lines, and redistributions of the oscillator strength between the pigments. Thus, NPHB, that is, light-induced shifts of the pigment transition energies, can result in changes in the whole picture of excitonic interactions. Such effects have indeed been observed in SPCS experiments on LH2 at low[19] or room[27−30] temperature. The important feature of such effects is that, because of the excitonic interactions, the redistribution of oscillator strength can occur quite far from the original spectral hole and even outside the wavelength range of the site distribution function of the state being burned. For example, we recently demonstrated that the exact character of this redistribution is quite sensitive to the assignments of the original site excitation energies of the chlorophylls in the CP43[31] and CP47[32] core antenna complexes of Photosystem II; in the case of CP43, the two lowest-energy states were assigned to particular chlorophylls, namely, Chls 37 and Chl 44,[31] using the Loll et al.[33] nomenclature. However, the antihole parameters used were free parameters of the model, and dispersive SHB kinetics was not taken into account in refs 31 and 32. Although the effects of the dispersive hole growth kinetics (HGK) on the nonresonant (low-fluence) holes discussed in refs 31 and 32 are expected to be fairly weak, refinement of this assignment might be in order (such research is in progress).

In summary, this article focuses on the shapes of the antiholes resulting from NPHB in the B800 band of the LH2 antenna complexes for which large amounts of single-complex data are available, as well as on the hole growth kinetics and homogeneous line/hole widths. These variables are discussed within the framework of the available theoretical models and compared, whenever possible, with SPCS results.

2. Materials and Methods

2.1. Spectroscopic Measurements. The choice of the light-harvesting system to be studied by means of SHB in this work was determined by the availability of single-complex data for comparison.[7,10,16,18−25] LH2 complexes from *Rps. acidophila* have been isolated and purified as described in ref 34. Immediately before the experiment (to avoid damage to the B800 band), the samples were mixed with glycerol at a ratio of 1:2 buffer/glycerol. This ensured the formation of high-quality transparent glass upon cooling. The 9-mm-thick plastic cuvette with this mixture was placed inside an optical cryostat (either by Janis or by Ukrainian Academy of Science) and quickly cooled to ∼5 K. The absorption spectra were measured with a Bruker FT-120 Fourier transform spectrometer at 0.5 or 1.0 cm^{-1} resolution (see figure captions). The holes were burned with vertically polarized light of a Coherent CR-899 Ti:sapphire laser with the MW (medium wavelength range, ∼780−890 nm) optics set and a bandwidth of several gigahertz (etalons out). Alternatively, holes were burned and scanned with a Spectra-Physics model 3900 Ti:sapphire laser with a bandwidth of <1 cm^{-1}; in this case, the stepper motor (ThorLabs) tuning the laser's birefrigent filter was calibrated using a HighFinesse Ångström WS-U30 wavemeter, and the transmitted light was detected with a Hamamatsu 7421-50 PMT/photon counter module and NI counter board. In these experiments, the sample was placed in an Eppendorf uvette. Burn times and intensities are given in the text and figure captions. The hole-burned spectra are postburn absorption spectra minus preburn absorption spectra. To avoid possible ambiguities caused by accounting for antihole absorption, the (resonant) hole widths in both experimental and theoretical spectra were defined as full widths at half-depth, with depth counted from zero. If holes had to be erased during the experiment, the sample had been heated in the dark to ∼150 K. After that, the absorption spectrum was measured to verify that the previous hole(s) has (have) indeed been erased and that no other spectral changes occurred.

The effects of the cuvette material on light polarization were explored. Laser light transmitted through the polarizer exhibited a degree of polarization $[(I_{max} - I_{min})/(I_{max} + I_{min})]$ of 95% (imperfections of laser and polarizer combined). Introduction of the uvette, which was used in the HGK measurements, reduced the degree of polarization to about 90% (after passing through two walls; obviously, the light interacted with the sample after passing through just one wall of the cuvette). Thus, the birefringence of the uvette material is negligible. The cuvette used in earlier measurements (with FTIR spectroscopy) exhibited much higher birefringence, with light exhibiting a degree of polarization of only about 30% after passing through the cuvette. In terms of the model described in the next subsection, burning and probing with partially depolarized light is equivalent to burning with polarized light but at lower power (a factor of 2 lower for completely depolarized light). Thus, as stated in the Experimental Results section, the irradiation doses used to obtain the hole spectra measured with the FTIR spectrometer were adjusted to achieve a match with the HGK data.

2.2. General Aspects of the Model Calculations. The frequency change in SHB in an amorphous solid is traditionally interpreted as being due to tunneling that takes place in an electronically excited state of a double-well potential: a two-level system (TLS). (See refs 3, 13−15, 26, and 35−37 and references therein; the applicability of this model to protein systems is discussed in section 4.) In the case of photochemical hole burning (PHB), the chromophore molecule has some bistable property (e.g., phototautomerization in the case of free-base porphyrins or phthalocyanines), whereas in NPHB, such a bistable system includes the pigment of interest together with its local environment (host matrix). During the NPHB process, the absorption eliminated (burned) at the resonant frequency is redistributed, and the hole spectrum is conservative. The frequency change mechanism for both types of SHB mentioned above is illustrated in Figure 1. Although it is based on schematics from refs 13−15, 26, and 35−37, our figure includes two hierarchical tiers of the energy landscape. At first, the system is in the electronic ground state; after the excitation, a finite probability exists for tunneling; and after electronic relaxation, the system will stabilize in the new configuration. Frequency change is persistent on the time scale of the experiment if the barrier is significantly higher in the ground state than in the excited state. The frequency change is caused by different asymmetries of the TLS in the ground and excited states. However, for both photochemical and NPHB mechanisms, the hole-burning rate-determining step is tunneling in the excited state, characterized by the tunneling parameter λ. $\lambda = d(2mV)^{1/2}/\hbar$, where d is the displacement along a generalized coordinate, m is the effective mass of the entity rearranging during the conformational change, and V is the barrier height.

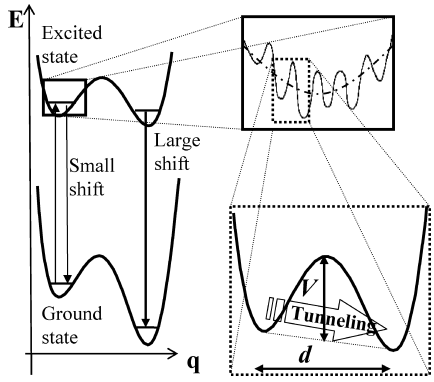

Figure 1. Mechanism of nonphotochemical spectral hole burning modified to account for different hierarchical tiers on the protein energy landscape. See text for details.

Because the chromophore interacts with an amorphous host, the tunneling parameter is subject to a distribution, which results in a broad distribution of HB rates $R = \Omega_0 \exp(-2\lambda)$[3,13−15,26,37] and renders SHB a highly dispersive (versus single-exponential) process. Because HGK can be described only numerically, all treatments neglect or approximate some aspects of this complicated process.[13−15,26,37] For example, in refs 13−15, the whole absorption spectrum time evolution was calculated without the inclusion of the NPHB antihole absorption, which allowed for the simulation of the evolution of narrow holes at low irradiation doses (over the first four orders of magnitude of doses) when the antihole is not the prevalent spectral feature. This condition is most easily satisfied when the width of the resonant zero-phonon hole is significantly smaller than the width of the antihole. However, for larger irradiation doses, the final hole shape forms in dynamic balance between an overlapping hole and its antihole, and therefore, a formalism was developed that also included the antihole absorption.[26] The latter model, which is called the "perfect-spectral-memory model" in the following discussion, allowed hole shape simulation with one set of parameters for increased irradiation doses. Light- and thermally induced hole filling was included in ref 37. The key assumption of the above models was that only a single ideal extrinsic TLS is realized on every chromophore. As irradiation doses increase further, the assumption of a single TLS for every chromophore ceases to work even in glasses, and one needs to include multiple TLSs with different tunneling characteristics and/or the realization of a multilevel system (MLS) on the same chromophore.[37,38]

The hole spectrum, $D(\Omega,t)$, is described by the SHB master equation,[14] which, in this article, was modified to include the distribution of the EET times, that is, $h(\tau_{EET})$

$$D(\Omega,t) = 1.5 \int d\omega\, L(\Omega - \omega, \tau_{EET})\, G(\omega) \int d\lambda\, f(\lambda) \times \int h(\tau_{EET})\, d\tau_{EET} \times \int d\alpha \sin\alpha \cos^2\alpha \times \exp[-P\sigma\varphi(\lambda,\tau_{EET})\, L(\omega_B - \omega, \tau_{EET}) t \cos^2\alpha] \quad (1)$$

Equation 1 describes the shape of the absorption spectrum after burning at ω_B with photon flux P for time t, with $G(\omega)$ being the site distribution function (SDF), which describes the probabilities of encountering different zero-phonon transition frequencies. Prior to any burning, SDF is described by a Gaussian. σ and ϕ correspond to the integrated absorption cross section of the molecule aligned with transition dipole parallel to laser polarization and the hole burning quantum yield, respectively. The NPHB yield can be defined by analogy with refs 3, 13−15, 26, and 37 as

$$\varphi(\lambda, \tau_{EET}) = \frac{\Omega_0 \exp(-2\lambda)}{\Omega_0 \exp(-2\lambda) + \tau_{fl}^{-1} + \tau_{EET}^{-1}} \quad (2)$$

where τ_{fl} and τ_{EET} are the fluorescence lifetime and EET time, respectively; λ is the tunneling parameter; and Ω_0 is a constant prefactor. $L(\omega_B - \omega,\tau_{EET})$ is the SSA profile with zero-phonon line (ZPL) at the burn frequency, ω_B, with ZPL width inversely proportional to the EET time. $f(\lambda)$ is the Gaussian distribution of the tunneling parameter with a mean of λ_0 and a standard deviation of σ_λ.

Two approaches can be employed for treating NPHB antiholes. If the chromophore is in interaction with one and only one TLS and therefore can assume only two spectral positions, one can follow the logic of ref 26. This approach is called the "perfect-memory model" in the subsequent discussion. Because LH2 SPCS results indicate that the single-molecule line can assume multiple spectral positions, the model corresponding to the opposite limiting case was developed and is referred to below as the "no-memory model". It was assumed that molecules starting at ω_{init} before burning are redistributed around ω_{init} according to a certain distribution, called the antihole function, as a result of burning. The sequence including burning for a small time and then recalculating $G(\omega)$ is repeated in a loop [index n below refers to the number of iteration; before any burn $G_0(\omega)$ is Gaussian]: The SDF of the burned molecules, $G_n(\omega)\{1 - \exp[-P t\sigma\phi L(\omega - \omega_B) \cos^2\alpha]\}$ is convoluted with the properly normalized antihole function and added to the postburn SDF $G_n(\omega) \exp[-P t\sigma\phi L(\omega - \omega_B) \cos^2 \alpha)$. This results in a modified shape of the SDF $G_{n+1}(\omega)$, without change in its normalization. Unlike in ref 26, there was no spectral memory, and no correlation was implied between the shifts of the absorption of a molecule in consecutive steps. The SHB yield was still determined by eq 2. Thus, one could argue that we were imposing undue limitations on the behavior of a single molecule by demanding that λ (the barrier height and width the given molecule is experiencing) would not change despite molecules sampling multiple nonidentical wells on the protein energy landscape. In fact, for our model to function as intended, it is sufficient that the total number of molecules experiencing a given λ at any given time does not change. In other words, the number of molecules diffusing into somewhat easier to burn conformations is assumed to be equal to the number of molecules diffusing into somewhat harder to burn conformations.

3. Experimental Results

Figure 2 represents a set of holes burned into the B800 band of the LH2 complex at 807.5 nm, that is, to the red with respect to the B800 band maximum. This ensures that the B800 molecules probed in this experiment are those incapable of B800 → B800 energy transfer and are subject to B800 → B850 energy transfer only.[34] The inset depicts the 5 K absorption spectrum of the LH2 complex. The complexes appear to be intact, as integral intensities of the B800 and B850 bands indeed scale as 1:2. For a shallow hole (I = 80 mW/cm^2 for 120 s, i.e., fluence of 10 J/cm^2, fractional depth of ∼5.6%), the ZPH width is 4.2 cm^{-1}, which corresponds to a B800 → B850 energy-transfer time of 2.5 ps, in agreement with SHB results reported earlier.[34,39−42] For the largest burn dose (810 J/cm^2), the width of the ZPH reaches ∼8.0 cm^{-1}, and the fractional hole depth reaches ∼40%. The observation of just 40% being burned for

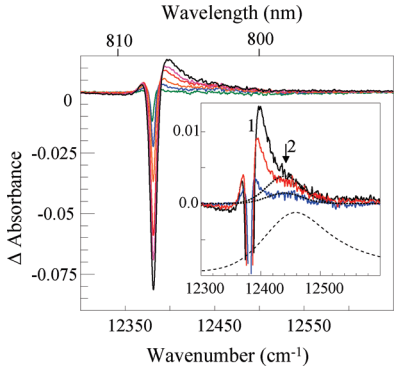

Figure 2. Spectral holes burned at 807.5 nm with various irradiation doses (9.5, 32, 79, 123, 443, and 808 J/cm^2). The inset shows a magnified region of the main plot with the focus on the NPHB antihole (and with the same color coding). The numerals 1 and 2 refer to different contributions to the NPHB antihole; see text. Dotted curves are the fit to the second, strongly shifted component of the antihole, also labeled with an arrow. The dashed curve is the B800 absorption spectrum.

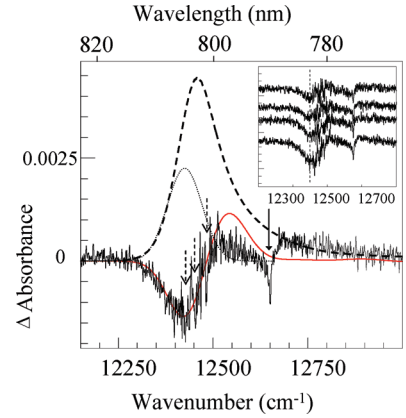

Figure 3. Nonresonantly burned hole spectrum obtained for $\lambda_B = 790.5$ nm, at ~150 J/cm^2. The dotted line is the fit to the SHB action spectrum, and the dashed line is the B800 absorption band (multiplied by a factor of 0.003). The thin red solid curve represents the hole due to EET and its antihole. Dashed arrows indicate vibronic replicas of the resonant hole. The inset contains nonresonantly burned hole spectra for different irradiation doses (50, 85, 100, and 150 J/cm^2, from top to bottom).

such a large irradiation dose is somewhat surprising, as the Huang−Rhys factor S is small for the B800 band (i.e., $S = 0.5$[23,25]) and the maximal fractional hole depth is expected to be approximately $\exp(-S) = 0.6$ when the hole is burned into the low-energy side of the absorption band. Possible explanations include light- and temperature-induced hole filling,[37] the influence of the SHB antihole (see below), and/or the geometry of the experiment. Regarding the latter possibility, the partially polarized light of the FT spectrometer is effectively probing the molecules with transition dipoles perpendicular to the vertical polarization of burning laser light as well. Alternatively, one could just suggest that some B800 molecules exhibit an exceptionally low hole burning yield. Further discussion on the issue of slow HGK is presented below.

Both real and pseudophonon sidebands (PSBs) are, except for the pseudosideband for larger irradiation doses, masked by the antihole due to the nonphotochemical nature of the hole burning. The antihole absorption, which is the main focus of this article, is obviously not uniformly distributed over the whole original B800 absorption band, but rather is distributed over a much narrower range both to the blue and to the red of the ZPH. It appears that, for all irradiation doses, the red fraction of the antihole approximately compensates the pseudo-PSB. The integral of the hole spectrum over a broad enough spectral range is close to zero, in agreement with the nonphotochemical nature of the hole burning process. Without turning to any particular model describing low-temperature light-induced dynamics of the system, one can characterize the hole spectra in Figure 2 by the gap between the centers of mass of the positive and the negative features of the spectra. The lowest-dose spectrum is almost perfectly symmetrical with respect to the burn wavelength. This is a signature of a combination of the weak electron−phonon coupling and the photoproduct shape centered on the burn wavelength. The antihole absorption is peaked at 10 cm^{-1} to the blue and to the red of the burn wavelength. Unfortunately, the signal-to-noise ratio of this shallowest hole spectrum does not allow for reliable determination of the integral intensities of the positive and negative features. For higher-dose spectra, the gap between the centers of mass of the positive and negative features gradually increases to ~60 cm^{-1}, with the antihole at higher energy with respect to the resonant hole. Upon examining the inset of Figure 2, where the hole/antihole region is enhanced, it is immediately apparent that the antihole exhibits quite complicated behavior even for relatively small irradiation doses. It is obvious that the experimentally observed antihole should be described with at least a two-peak distribution. Whereas the first peak is located in the vicinity of the original hole, the second one is shifted much farther to the blue, as indicated by the downward pointing solid arrow. It can be demonstrated that, for a realistic shape of the PSB and a value of the Huang−Rhys factor S on the order of 0.5, the latter peak cannot be attributed solely to the real phonon sideband of the first peak. One could also note that, for medium and large irradiation doses, the second peak (labeled 2) of the antihole near ~12460 cm^{-1} does not develop as fast as the first one (labeled 1); that is, it most likely saturates for relatively low irradiation doses, with the further slow increase of absorption around 12460 cm^{-1} most likely being due to the phonon sideband of peak 1. This means that large spectral shifts resulting in the formation of antihole peak 2 are experienced only by a small fraction of molecules, but the SHB yield for this small fraction is, on average, larger than that for the molecules forming antihole peak 1. Finally, it is worth mentioning that the parameters of the antihole illustrated by peak 2 (dotted Gaussian curve) are still significantly different from those of the whole B800 band (dashed curve). This indicates that the largest spectral shifts still do not result in redistribution of the molecules' absorption over the whole B800 band.

Another type of hole burning experiment involves burning at the higher-energy side of the B800 band and observing the satellite hole structure resulting from B800−B800 energy transfer. The result of burning at 790.5 nm is depicted in Figure 3; other burn wavelengths at the blue edge of the B800 band were also used (data not shown for brevity). The B800 molecules absorbing at this wavelength (790.5 nm) are the highest-energy pigments in the B800 ring, and therefore, they are capable of not only B800 → B850 but also B800 → B800 EET. As a result of the latter process, both the hole burning yield and the induced absorption rate at resonance with the laser are significantly reduced, but a broad hole is formed at lower energies within the B800 band. The shape of the entire hole-burned spectrum is fairly complicated, as it includes resonantly burned ZPH at 790.5 nm, its real and pseudo-PSBs, and the antihole absorption distributed in the vicinity of the resonant hole (as in the case of Figure 2), as well as the nonresonantly burned broad low-energy hole and its antihole. Some of these features overlap, which further complicates the analysis. One should also note that sharp

satellite holes (indicated by the dashed arrows) at 168, 197, and 224 cm^{-1} (with respect to the resonant ZPH) are vibronic replicas (i.e., ZPLs burned through vibronic bands due to intramolecular vibrations)[43] and are not a part of the broad feature due to B800 → B800 energy transfer. It appears, as expected, that these vibronic holes are accompanied by narrow antihole positive spikes between the vibronic holes.

The key observation in the case of nonresonant burning is that the antihole of the broad hole due to the B800 → B800 energy transfer is strongly blue-shifted with respect to the broad hole itself. Assuming that the SDF of the burned fraction of the B800 band can be described with the same curve as the SHB action spectrum taken from ref 34 and indicated by the dotted Gaussian in Figure 3 (see also the Discussion and Simulations section for parameters) and that the antihole SDF of that broad hole is also Gaussian in the first approximation, one can roughly estimate that the average shift of transition energies of pigments burned within the B800 band (i.e., the shift of the burned B800 absorption lines) is approximately 60−70 cm^{-1}, in agreement with the data in Figure 2. The red derivative-like curve in Figure 3 is the sum of these two Gaussians, a lower-energy one (broad hole centered near 12430 cm^{-1}) for the initial absorption that was burned and a higher-energy one for the antihole absorption. Interestingly, the area of the former Gaussian is just 0.17% of the area under the B800 band, or 0.5% of the integral intensity of the absorption of B800 molecules incapable of the B800 → B800 energy transfer and, therefore, more prone to spectral hole burning. Increasing the irradiation dose from ∼150 to ∼300 J/cm^2 [at 791.8 nm, where the optical density (OD) is slightly higher and, therefore, the fraction of absorbed photon flux is also higher] resulted in just a 20% increase in the integral intensity of the burned band (other parameters of the band could stay the same and still result in a good fit). This indicates that the position of the broad feature near 12430 cm^{-1} is not correlated with the burn wavelength, in agreement with this broad hole being due to energy transfer. Such behavior also indicates that the fraction of B800 molecules experiencing large spectral shifts in this experiment is quite small. It needs to be stressed that the shape of the broad nonresonant hole and its antihole in Figure 3 is only weakly dependent on the irradiation dose (see the inset of Figure 3), which, in turn, suggests that the feature is formed as a result of one large spectral shift per each individual B800 molecule line rather than as a result of many small shifts. Otherwise, one would expect gradual migration of the derivative-like hole/antihole feature to higher energies.

Figure 4 depicts the evolution of the spectral hole burned at 12376.2 cm^{-1} (808 nm) and read with a resolution of 0.5 cm^{-1} within the first 45 min after the end of a moderate burn resulting in about a 15−20% decrease of the resonant absorption. Both holes are 4.9 cm^{-1} wide, and within the experimental uncertainty, no broadening was observed. On the other hand, hole filling was quite prominent, as only about 70% of the original hole remained intact after 45 min. This intense filling is induced by the white light of the Fourier transform spectrometer. Holes similar to those depicted in Figure 4 did not exhibit significant filling after 2 h in the dark [these holes were measured using low-intensity (∼10 $\mu W/cm^2$) laser scans in transmission mode instead of the FTIR spectrometer]. The combination of negligible broadening; significant white-light-induced hole filling; and much slower, if any, filling in the dark indicates that the hole spectrum and its evolution are the result of single B800 lines (which are contributing to the hole) experiencing shifts between

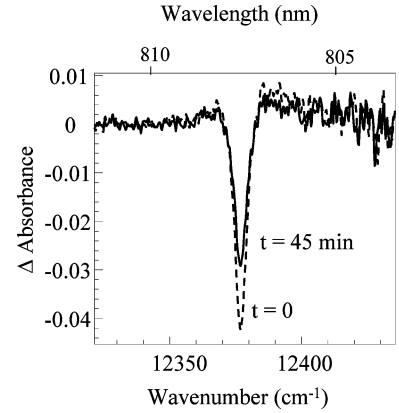

Figure 4. White-light-induced hole filling. The spectral hole burned at 808.0 nm was recorded immediately after being burned (dashed line) and 45 min later. Resolution = 0.5 cm^{-1}, T = 5 K.

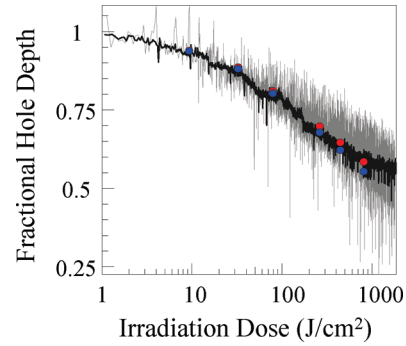

Figure 5. HGK curves obtained at 0.23 W/cm^2 (0.5 s/point; dark gray curve) and 1.37 W/cm^2 (0.1 s/point; light gray curve) at 807.5 nm, as well as hole depths extracted from the spectral holes in Figure 2 (circles). The upper (red) circle of each pair corresponds to data as measured; the lower (blue) circle corresponds to data corrected for white-light-induced hole filling at the rate in agreement with Figure 4.

a small number of spectral positions per line. Moreover, these spectral positions are well separated from each other, specifically, by a frequency interval that is larger than the hole width. The availability of multiple spectral positions per line close to the original hole would result in broadening accompanying light-induced filling, but such broadening is not observed.

Figure 5 shows the HGK data obtained at 807.5 nm. The solid noisy curve represents the HGK curve obtained for a burning intensity of 0.23 W/cm^2. The noisier gray curve corresponds to a burn intensity of about 1.37 W/cm^2. Within experimental uncertainties, the curves are similar, indicating that the HGK does not significantly depend on the burn intensity within that range. The absence of additional fast components (vide infra) of SHB kinetics was assured in two independent ways. First, the HGK curves were measured for shorter periods of time with burn intensities reduced to 0.05 and 0.01 W/cm^2. These curves match the curves (i.e., at the beginning of hole evolution) depicted in Figure 6; data not shown for clarity. Second, it has been confirmed that the change of absorbance that can be calculated based on the HGK curves is, within experimental uncertainty, equal to that obtained from the hole spectra measured after the measurements of the HGK: $I_{beg}/I_{end} = I_{preburn}/I_{postburn} = 10^{OD_{end}-OD_{beg}}$, where I_{beg} and I_{end} are the transmission signals at the beginning and end, respectively, of the HGK measurement; $I_{preburn}$ and $I_{postburn}$ are the transmission signals at the burn wavelength in the unprocessed hole spectra; and OD_{beg} and OD_{end} are the respective optical densities. Thus, we conclude that there are no fast burning or filling processes

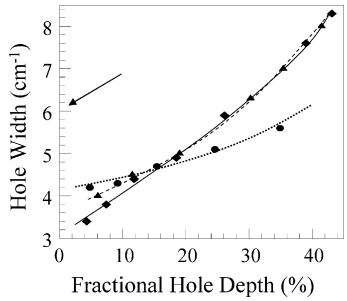

Figure 6. Experimental dependence of the hole width on the fractional hole depth (▲, − − −), predicted dependence in the absence of a homogeneous line width distribution (●, • • •), and predicted dependence assuming the distribution of line widths from ref 4 (♦, —). See Table 1 for other parameters. All lines are guides for the eye only. The value of the (shallow) hole width expected based on the time-domain data (i.e., about 6 cm^{-1}) is indicated by an arrow; see text for details.

(transient holes) affecting the holes measured with the FT spectrometer (aside from the relatively slow white-light-induced filling depicted in Figure 4). Data obtained from the holes reported in Figure 2 are superimposed on the HGK curves. Each hole from Figure 2 is represented by a pair of circles in Figure 5. The upper circle (in red) corresponds to the hole depth as measured, whereas the lower circle (in blue) corresponds to the hole depth expected in the absence of white-light-induced filling, in agreement with data shown in Figure 4. In view of the difficulty in determining the state of polarization and intensity of light used to burn and to record the holes reported in Figure 2, the irradiation doses used to burn these holes were systematically adjusted in such way that the hole depths would match the HGK curves in Figure 5 (there was much better control over burn intensity in the HGK measurements).

4. Discussion and Simulations

4.1. Excited-State Tunneling versus Ground-State Barrier Hopping. We start with an overview of the models describing protein dynamics in general and the phenomena observed in SHB and SPCS experiments in particular. The goal is to convince the reader that the model involving excited-state tunneling described in section 2.2 is indeed applicable to chromophores embedded in a protein. The key issue complicating a direct comparison of the results of various types of experiments is that different experiments probe related but different phenomena. Specifically, the waiting and aging time SHB experiments by Friedrich's group (see ref 17 for review) probe spectral diffusion and the distribution of energy barriers in the dark, that is, in the electronic ground state. On the other hand, SPCS experiments[7,10,16,18−25] probe light-induced spectral diffusion, which, we believe, is essentially the phenomenon responsible for NPHB and which most likely occurs due to phonon-assisted tunneling processes in the excited electronic state.

An alternative NPHB mechanism involving TLS was proposed by Bogner and Schwarz.[44] In that model, hopping over the barrier occurs in the electronic ground state (see Figure 1), using the thermal energy provided by radiationless decay of the electronic excited state. A discussion on the applicability of the above model to glasses can be found in ref 45. It appears that, in refs 16 and 17, in an analysis of spectral diffusion data in a protein obtained by SPCS, it was implied that a mechanism similar to that of Bogner and Schwarz might be operational. For instance, it has been argued that the fluorescence quantum yield of LH2 is 10% and that the dissipated thermal energy is large enough to cause jumps between the ground-state conformational states of the protein. One could expect B800 → B850 energy transfer to be accompanied by excitation of bacteriochlorophyll *a* (Bchl *a*) intramolecular modes in the range of ∼900 cm^{-1}.[43,46] Thermal energy of this magnitude would be sufficient to facilitate hopping over the barrier in the electronic ground state if the localized Bchl *a* vibrations were sufficiently strongly coupled to movements responsible for conformational changes. However, in this scenario, the B800 SHB yield ϕ (eq 2) would not depend on the excited state lifetime and should not be affected by the fast B800 → B800 excitation energy transfer, contrary to the experimental observations[34,41] and the predictions of the excited-state tunneling model, where EET and NPHB are competing processes. The independence of the SHB yield from the EET time clearly contradicts all known experimental results on SHB in photosynthetic complexes.

Interestingly, very recently, experimental evidence has been presented that, although the probabilities of frequency shifts in LH2 SPCS experiments are temperature-independent (i.e., supposedly due to tunneling) in some cases, in other cases, the shifts could be thermally activated and, therefore, ascribed to barrier hopping, which is not even indirectly light-induced.[24] According to ref 24, those B800 lines that exhibited temperature-dependent behavior experienced spectral shifts larger than 5 cm^{-1} within minutes at 5 K, independently of excitation intensity. The idea that the B800 line shifts are not light-induced clearly contradicts the lack of hole filling in the dark at 5 K for hours, which we reported above with reference to data shown in Figure 4. We suppose that the experimental setup described in ref 24 could be prone to local sample heating by the laser beam, especially at temperatures above 4.2 K, when the sample was not in liquid helium. Also note that, according to ref 37, the tunneling rate might be temperature-dependent, and therefore, the presence of a temperature dependence of the probability of line shifts cannot be used as an argument against tunneling. In summary, we believe that tunneling in the excited state is the mechanism responsible for both NPHB and shifts of the spectral lines in SPCS experiments and that a model properly treating tunneling in MLS, with more than one hierarchical tier, needs to be considered to explain the results of both types of experiments (such research is in progress). Meanwhile, we can use available data and attempt to determine some parameters relevant for the development of a protein SHB model.

4.2. Hole/Line Widths. The observed widths of the spectral holes or SPCS lines in LH2 are determined by the EET times and by the spectral diffusion occurring in steps smaller than the hole width and at a time scale faster than the time scale of the experiments. Therefore, in this subsection, we limit ourselves to the fastest (smallest, i.e., spectral shifts of a couple wavenumbers or less) tier(s) of the protein energy landscape and compare the homogeneous line widths resulting from our SHB experiments and low-temperature time-domain experiments[42,47,48] with the SPCS results obtained by Köhler's group.[7] The fact that our data were obtained for *Rps. acidophila* whereas ref 7 focused on *Rb. sphaeroides* should not be a significant impediment to this part of our analysis. That is, it has been already demonstrated through time-domain experiments[42,47,48] that LH2 from *Rps. acidophila, Rb. sphaeroides*, as well as from *R. molischianum* have similar average B800 → B850 energy-transfer times (at liquid helium temperature) on the order of about 1.5−1.7 ps. The latter corresponds to a homogeneous line width of 3.0−3.4 cm^{-1} (or a zero-dose hole width of 6.0−6.8 cm^{-1}). Very recently, it was reported that the SPCS line shift

TABLE 1: Parameters of the Best Fit to the HGK and Hole Shape Data[a]

phonon sideband	$S = 0.45 \pm 0.05$, $\omega_{peak} = 25$ cm^{-1}, Gaussian/Lorentzian fwhm of 22/40 cm^{-1}
homogeneous line width	distribution from ref 4 based on the whole B850 DOS, peaked at 3.3 cm^{-1} (1.6 ps)
antihole, tier 1, shifts ~1 cm^{-1}	$\phi > 10^{-6}$, $\lambda_0 \leq 7.8$, $\sigma_\lambda \leq 0.1$; not observed in SHB experiments
antihole, tier 2, shifts ~7−10 cm^{-1}	fwhm = 35 ± 5 cm^{-1}, shift = 3 ± 1 cm^{-1}, $\lambda_0 = 10.3 \pm 0.2$, $\sigma_\lambda = 0.7 \pm 0.2$ ($\phi \approx 10^{-8}$)
antihole, tier 3, shifts ~60 cm^{-1}	fwhm = 70 ± 10 cm^{-1}, shift = 60 ± 10 cm^{-1}, $\phi \approx 10^{-7}$; note that only several percent of molecules are capable of such large shifts

[a] Model with no spectral memory.

probability distributions are very similar for LH2 complexes from all three organisms.[25] Thus, similar line-width-related properties are expected for LH2 from all three organisms. We note that smaller hole widths were obtained in SHB experiments in this work and in ref 40, which can be explained by SHB, in a shallow-hole regime, predominantly probing the longer-lifetime (narrower-line-width) edge of the lifetime distribution, in the case the latter is present. (This is another manifestation of the SHB yield being dependent on the energy-transfer rate.) Interestingly, both the line widths observed in SHB and those calculated from the results of time-domain experiments are smaller than the line widths obtained in the recent SPCS experiments. It was reported in ref 7, for example, that the line width near 12390 cm^{-1} (807 nm), on the red side of the B800 band, of one and the same molecule exhibited variations from scan to scan with a(n) (asymmetrical) distribution peaked at ~4 cm^{-1} and with a width of 8 cm^{-1}. The parameters of that distribution appeared to be intensity-independent between 5 and 15 W/cm^2 (circularly polarized light), which indicated that the single complex line being followed did not experience saturation broadening. The peak (or center-of-mass position, because the spectral moment/cumulant approach was employed in ref 18) of the single B800 molecule line also fluctuated from one SPCS scan to another. Such fluctuations were described statistically in two different complementary ways. First, the distributions of line shifts between two consecutive scans were presented in refs 18 and 25. These distributions were clearly dominated by the smallest, ~1−2 cm^{-1}, shifts. Second, the distribution of the first cumulant,[7,18] or spectral diffusion kernel, was reported. In the latter case, the information about the particular sequence of shifts leading to the cumulant distribution is lost, but one can determine the spectral position(s) at which the line spends the most time. The first cumulant distributions consisted of one or more Gaussians with widths on the order of 10 cm^{-1}, separated by 7−8 cm^{-1}. Whereas the former number describes the fast diffusion due to small, ~1 cm^{-1} shifts, the latter reflects the average magnitude of the shifts on the next tier (7−10 cm^{-1}) of the protein energy landscape.

The B800 → B850 EET mechanism is not fully determined. Models based on a classical Förster approach result in poor agreement between predictions and experiment. The so-called modified Förster approach,[4−6] where the whole B850 density of states (DOS) is considered rather than just the allowed energy levels, results in a broad distribution of EET rates peaked at values agreeing with the results of the time-domain experiments. Figure 6 depicts the experimental dependence of the hole width on the fractional hole depth at 807.5 nm (triangles) and the results of simulations assuming the absence of the distribution of EET rates (circles). (A series of holes burned at the same frequency with different doses was simulated, and their widths and depths were measured. The single homogeneous line width employed was 2.2 cm^{-1} to ensure that the hole width dependence extrapolated to ~4 cm^{-1} at zero dose, in agreement with the experimental HB results.) Comparison of the data represented by the circles and triangles in Figure 6 reveals that the hole broadens much faster than expected in the single-line-width case (see the circles), suggesting the presence of some B800 → B850 EET rate distribution that should be incorporated into advanced modeling as discussed below. We employed the distribution of EET rates from ref 4. The dependence of the hole width on fractional hole depth resulting from use of the latter distribution (see the diamonds) is depicted in Figure 6 for comparison. (Details on other parameters used to produce the theoretical data are discussed later.) We should stress that the distribution from ref 4 is "static", with different B800 molecules exhibiting different B800 → B850 EET rates that do not change in time. The distribution of line widths resulting from the SPCS experiments, on the other hand, is "dynamic", meaning that the same molecule seems to undergo continuous changes of the homogeneous line width. In principle, one could reconcile the two distributions (if only qualitatively, as their quantitative parameters still differ) by assuming that spectral diffusion for B850 molecules is much faster than that of B800 molecules and results in much larger shifts translating into large changes of the B850 DOS. However, the dynamic distribution with such parameters is not compatible with the absence of hole broadening depicted in Figure 4. With respect to Figure 4, one should also note that the absence of noticeable broadening of the hole depicted in this figure is inconsistent with spectral diffusion of the magnitude observed in SPCS experiments and reflected by the first cumulant distributions,[18] occurring in the dark (note, here it does not matter whether this dark diffusion involves ground-state tunneling or barrier hopping). We emphasize that the discrepancy between the widths of the first cumulant distributions (SPCS) and of the hole in Figure 4 cannot be attributed to different time scales of the experiments, as in SPCS experiments,[7,18] many tens of scans were taken within the first couple hours of the measurement. Consequently, we suggest that the widths of the lines observed in recent SPCS experiments are a result of narrower lines exhibiting spectral shifts within the time necessary to traverse a several-wavenumbers-broad line in an SPCS excitation spectrum scan; additional arguments to support the above statement are presented below,

4.3. Photon Budgets. Before proceeding further, we estimate the number of excitations per unit time that B800 molecules experience in SHB and SPCS experiments. We assume that the spectral fluctuations observed in both experiments are light-induced and, therefore, that the rate of these fluctuations should

depend on the photon flux/excitation intensity. (We are aware that the above statement appears to contradict the fluence independence of the results of refs 10, 18, and 19, and we will comment on that shortly.) First, we hasten to stress that this line of reasoning is independent of whether tunneling or barrier hopping is at work: The more often the system is excited, the larger fraction of the total time it spends in the states from which either tunneling or barrier hopping is possible. According to Alden et al.,[49] the peak molar absorption coefficient of LH2 from *Rps. acidophila* at 120 K near 800 nm is 3.8×10^6 $(M_{LH2})^{-1}$ cm^{-1}, which corresponds to a 5 K peak absorption cross section of an individual B800 molecule with its transition dipole parallel to a light electric field of about $(1.2-2.3) \times 10^{-13}$ cm^2 for homogeneous ZPL widths of 4 cm^{-1} (SPCS) and 2 cm^{-1} (SHB) and $S = 0.5$.[23,25] For an excitation intensity of 10 W/cm^2 (circularly polarized light) and an average ZPL width of 4 cm^{-1} (SPCS), about 4 500 000 photons are absorbed per second while the spectral line is resonantly excited (which is obviously not enough to cause undesirable saturation in the case of a ~2-ps excited-state lifetime). The number of photons estimated above also considered the fact that, because of interpigment interactions within the B800 band, the lowest-energy B800 states have an oscillator strength of ~1.5 Bchl *a* equivalents. (The latter number was also used in subsequent modeling of the hole-burned spectra.) The 4 cm^{-1} wide line was traversed in ~0.1 s in single-molecule spectroscopy (SMS) experiments, resulting in roughly 450 000 photons being resonantly absorbed by each B800 molecule in one scan at 10 W/cm^2 excitation intensity. (The same estimate can be made by noticing that the line width of 2 cm^{-1} yields the same number of photons per scan, as the integrated absorption cross section remains the same.) Taking into account the ~10% fluorescence quantum yield of LH2 and the several percent collection/detection efficiency of the SPCS setup,[7,18,19] this estimate is in reasonable agreement with the observed integrated intensities of several thousand photons per line in the single-scan SPCS spectra.[7,18,23] As argued in the previous subsection, the (dynamic) SPCS distributions of the line width and position observed in ref 7 or thermally activated character of spectral diffusion are incompatible with the absence of appreciable hole broadening (see Figure 4). Thus, the line width distributions[7] most likely are a consequence of a line, narrower than the average SPCS line width (i.e., in better agreement with the time-domain or SHB results), experiencing small light-induced fluctuations that are faster than the characteristic time scale of the SPCS experiment, that is, faster than 0.1 s for excitation intensity of 10 W/cm^2. One should note that the independence of the fast spectral diffusion behavior from the excitation intensity reported in SPCS experiments might be a result of the probability of a single light-induced fluctuation being so high that, within the characteristic time scale of the SPCS experiments,[18] the molecule can sample most of the conformations available on this lowest-barrier tier of the protein energy landscape for any excitation intensity used in SPCS experiments,[10,18,19] that is, any intensity larger than 5 W/cm^2. In other words, $1/450\,000 = 2.2 \times 10^{-6}$ could be the lower limit of the probability of a single light-induced fluctuation resulting in a line shift of a few wavenumbers or less, and the chromophore molecule samples more than just two positions on the energy landscape per SPCS scan. Assuming the same prefactor value of $\Omega_0 = 7.6 \times 10^{12}$ s^{-1} as is usually employed for glasses (use of different prefactor just shifts the mean of the λ distribution), the upper limit for the tunneling parameter distribution mean λ_0 for this tier becomes ~7.8, comparable to that observed in glasses.[13-15,26,37] However, in view of the above discussion on the intensity independence of spectral diffusion behavior, it is feasible that the real λ_0 value could be lower.

The maximal excitation intensities employed in our SHB experiment (1.4 W/cm^2, linearly polarized light) were quite comparable to those used in SPCS. For this intensity, every B800 molecule in resonance with the laser absorbs $\sim 1 \times 10^6$ photons per second (or more if it is taken into account that lower-energy B800 states are borrowing oscillator strength from the higher-energy ones), and the fact that the small-range spectral line shift probability is larger than 1/450 000 makes the (small) frequency shift of a given molecule very likely even for burn times of just 1 s, and practically inevitable in hundreds of seconds as in our SHB experiment. This, in turn, should result in extremely fast hole burning in the case when the burned molecules never return to their preburn original wavelengths. To ensure agreement with the data shown in Figure 2, one would have to require that multiple back-and-forth small fluctuations make the probability of a single SHB event (line shift) possible; that is, the SHB yield ϕ would have to appear much smaller than it actually is (i.e., >1/450 000).

Concerning the shape of the nonresonantly burned spectral hole and its antihole (Figure 3), one should note that the formation of this combination of spectral features requires the blue shift of the B800 molecules absorption to be quite large. One can again estimate the number of photons absorbed by the system and the number of excitations redistributed by B800 → B800 energy transfer to the lower-energy B800 molecules. For the largest irradiation dose, about 150 J was delivered to the illuminated part of sample volume. (The Ti:sapphire laser was operated with MW optics set, so the maximal power at 790 nm was much lower than that at 807 nm.) With OD an of ~0.1 (790.5 nm; the weak contribution from vibrations building up on the B850 band were excluded), 21% of this energy was absorbed by the higher-energy B800 molecules in resonance with the laser. That is, about 8.4×10^{19} excitations eventually passed through one-third of the B800 molecules that were incapable of B800 → B800 energy transfer.[34] [These excitations passed through other B800 molecules as well. We just assume that, for these molecules, the SHB yield is several times lower (see eq 2) and ignore their contribution to SHB, to a first approximation.] The total number of Bchl *a* molecules in the excited volume of ~150 mm^3 is about 10^{14}, utilizing the same molar extinction coefficient as used by Alden et al.[49] Thus, every low-energy B800 molecule in our sample was excited about 2.5×10^6 times before the hole structure depicted in Figure 3 was formed. In addition, as follows from the hole magnitude analysis, about 0.5% of these molecules actually experienced large light-induced blue spectral shifts.

In the case of the SPCS experiment involving measurement of the fluorescence excitation spectrum of the B800 region, the lower-energy molecules also can become nonresonantly excited through B800 → B800 energy transfer after the higher-energy molecules are excited resonantly. For a constant scan speed, a single B800 molecule on the low-energy side of the band most likely is excited by energy transfer several times more frequently than it is excited resonantly (obviously, this factor should not be larger than 7-8, depending on the species). In this respect, the fluorescence excitation SPCS experiments are more similar to the nonresonant SHB experiments (Figure 3), than to the resonant ones (Figure 2). One can estimate that every low-energy B800 molecule is excited, both resonantly and by energy transfer, about 2×10^6 times per SPCS scan at 10 W/cm^2. Hofmann et al. reported the rates of large line shifts and intensity redistributions involving several lines (essentially large shifts

accompanied by excitonic effects) in the range of 0.0005−0.012 s^{-1}.[19] However, these shift rates were just the inverse of the average time between the line shifts, of 2000 and 80 s, respectively, without reference to the scanning rate or the illumination intensity. Because we believe that the spectral shifts are light-induced, it appears to us to be more informative to consider the shift rates expressed in terms of number of shifts per number of excitation events. Based on the data presented in refs 19 and 23, one can conclude that the above rates correspond to $(57-2 \text{ scans})^{-1}$ or, with an excitation intensity of 10 W/cm^2, to between 100 million and 4 million excitations (resonant and nonresonant) per large spectral shift. Because large shifts were not observed in many complexes within the time of the experiment, this range probably should be further extended to even higher values. Thus, the probability of large shifts (∼100 cm^{-1}) is at least 7−150 times lower than the probability of the smallest, ∼1 cm^{-1} ones. This again is in agreement with the idea that the mechanism causing the broad low-energy hole in Figure 3 is a result of one, not many, large jumps per B800 molecule involved.

It is interesting to note that, in the published SPCS data (up to 7000 scans in ref 23), the lower-energy lines did not exhibit any obvious preference for either large shifts or slow systematic creep to the blue. In ref 19, two out of three molecules exhibiting large spectral shifts actually preferred to occupy the conformation with lower, not higher, transition energy. For two complexes where correlated shifts of several lines have been reported, one preferred to be in the conformation with the center of mass of the spectrum shifted to the blue, and another preferred that to the red. All that despite the fact that, as mentioned above, lower-energy molecules are actually more frequently excited through B800 → B800 energy transfer! One reason to expect the blue-shift tendency in any frequency-domain experiments on B800 is obvious: In the case of a large enough blue spectral shift, the respective molecule most likely ceases to be the lowest-energy B800 molecule incapable of B800 → B800 energy transfer, its excited-state lifetime shortens several times, its ZPL width correspondingly increases, and both its induced absorption rate and HB yield decrease. As a result, the blue-shifted molecule and its surroundings might get "trapped" in the conformational state with the higher transition energy. Note that the negligible dose dependence of the distance between the broad burning band and its antihole in the nonresonant SHB spectra (see inset of Figure 3) also indicates that all small (several to ∼10 wavenumbers) spectral shifts to the blue and to the red are nearly equally probable. The small magnitude of the shift makes the trapping of complexes in the higher-transition-energy configuration (by increasing lifetime and decreasing HB yield as described above) unlikely for these tiers of the energy landscape.

4.4. Hole Simulations. Guided by the arguments presented in the previous sections, we attempted to fit the holes in Figure 2 and the HGK curves in Figure 5 with a modified SHB model including antihole absorption (no-memory model; see section 2.2). The ultimate goal of this analysis is to obtain a set of parameters that allows for satisfactory fitting of all of the holes in the series, with burn times and intensities scaling as those in the experiment. The list of these parameters includes the peak and mean of the tunneling parameter distribution and the shapes of the phonon sideband and of the antihole distribution. Based on the results of ref 34, we assumed that the absorption spectrum of the B800 molecules capable of only B800 → B850 energy transfer and therefore most easily experiencing hole burning was represented by the HB action spectrum, which is peaked at 12425 cm^{-1} (804.8 nm) (to the red of the B800 band maximum) and has a width of 108 cm^{-1}; see Figure 3. Therefore, the hole at 12381 cm^{-1} was burned 44 cm^{-1} to the red with respect to this sub-band maximum. (However, because the burn wavelength is located at the red side of the B800 band, the choice of the SDF parameters is not very critical as long as that SDF provides a good fit to the red side of the band.) The initial guess values for phonon sideband parameters were set to produce single-site absorption (SSA) spectra resembling those in refs 23 and 25. No data have been reported so far indicating that the parameters of the phonon sideband (or distributions of these parameters[23,25]) are strongly wavelength-dependent in the case of the B800 band of LH2. Although strong wavelength dependence of electron−phonon coupling was observed in some systems,[50] for states localized on a single pigment in photosynthetic antennae (within one band), this dependence is usually weak.[51,52] Two-component fluorescence, with these two components exhibiting significantly different electron−phonon coupling, has been observed for LH2 and LH1 antenna complexes.[53,54] However, this effect results from the coexistence of large and small exciton polarons in the ring of very strongly interacting pigment molecules, a situation that is dramatically different from that of the B800 band. The presence of a relatively narrow distribution of the PSB parameters[25] provides a negligible contribution to the dispersion of SHB kinetics (data not shown). The same is also true for the distribution of oscillator strengths (obtained from excitonic calculations on nine Bchl *a* molecules of the B800 ring); the mean value of the oscillator strength corresponds to the equivalent of about 1.5 Bchl *a* (see section 4.3). Thus, both of these distributions were neglected to accelerate the calculations. For calculated hole growth curves and spectra, a broad variety of shapes of the antihole function (see section 2.2) was tested, including Gaussian and Lorentzian functions peaked at zero with respect ω_{init}, slightly blue-shifted Gaussian and Lorentzian functions, and two-component antihole functions corresponding to the situation when the molecules can also experience large spectral shifts but with smaller probability. The latter approach is more appropriate than a two-peak tunneling parameter distribution in a situation when the same molecule is capable of both small and large shifts. The results of simulations are presented in Figure 7. Figure 7A represents the experimental data (error bars) and calculated HGK (smooth curves) obtained for $\lambda_0 = 7.8$ (upper limit for the small-shift tier of the protein energy landscape according to the photon budget arguments discussed above), $\sigma_\lambda = 0$, and various shapes of the antihole function. Solid curve a, representing a good fit to the experimental data, was obtained using a nonshifted Gaussian antihole function with a width of 1.1 cm^{-1}. Curves b and c in Figure 7A were obtained assuming the presence of larger (∼10 cm^{-1}) shifts in addition to small (i.e., ∼1 cm^{-1}) ones. In case b, the relative probability of the large shifts was assumed to be 0.025, which corresponds to $\lambda_0 = 9.6$ for the next tier of the energy landscape, and in case c, that probability was assumed to be 0.05 (next tier $\lambda_0 = 9.2$). Curve d was obtained for a nonshifted Lorentzian antihole function with a width of 1.1 cm^{-1}. The use of a small, < 0.1, value for σ_λ is justified by the argument that the parameters of the adjacent wells on this smallest-barrier tier of the energy landscape cannot vary much from well to well (see also refs 16 and 17). Increasing σ_λ results in HGK becoming more dispersive but not slower on average, so a significant increase of σ_λ would make agreement between calculations and experiments even worse. For experimental data points, as in Figure 5, the error bar was determined for the upper limit (smaller Δ absorbance) by results directly extracted from experimental data shown in Figure 2 and for

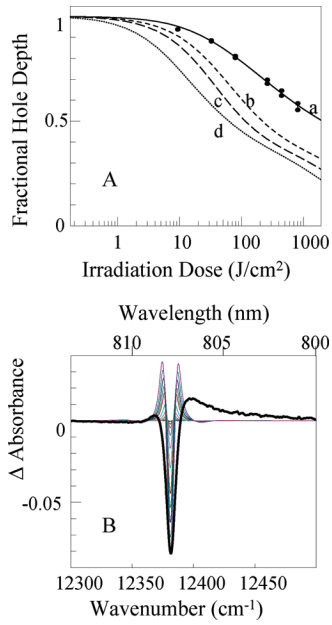

Figure 7. (A) Circles/bars represent experimental dependence of the hole depth on irradiation dose. (a) Best-fit HGK curve calculated for nonshifted Gaussian antihole function with fwhm = 1.1 cm^{-1} and λ_0 = 7.8 (solid curve). (b,c) Cases for which, in addition to fast burning with the same parameters as for curve a, the molecules can also experience larger shifts with relative probabilities of 0.025 and 0.05, respectively. (d) Nonshifted Lorentzian antihole function with a width of 1.1 cm^{-1} and zero probability of large shifts. (B) Deepest spectral hole burned at 807.5 nm (bold solid curve), as well as spectral holes calculated for several burn doses for $\lambda_0 = 7.8$ and Gaussian antihole function with fwhm = 1.1 cm^{-1} centered at ω_{init} (thin colored curves).

the lower limit by the same data but corrected for hole filling according to Figure 4. As can be seen, it turns out that, for this range of λ values, one can successfully fit the experimental HGK only by assuming that the antihole function is a single nonshifted Gaussian that is very narrow, ~1.1 cm^{-1} fwhm, in disagreement with the reported SPCS data (see Figure 1 in ref 18). Reduction of the tunneling parameter mean λ_0 below 7.8 results in a further decrease of the antihole distribution width required to fit the SHB kinetics. Any antihole models allowing even a small fraction of the molecules to escape farther from the excitation energy than a fraction of a wavenumber resulted in the calculated HGK becoming too fast. Figure 7B demonstrates that the use of the antihole shape parameters allowing for successfully fitting the HGK at $\lambda_0 = 7.8$ results in extremely poor fits for the overall hole shapes. Note that all of these curves were produced with the line width (EET rate) distribution being turned off, as turning it on for this range of λ values resulted in hole burning kinetics becoming too dispersive even for $\sigma_\lambda = 0$ (data not shown). Also, including the line width distribution did not result in any significant improvement of the hole shapes in Figure 7B. Thus, we conclude that single complex lines reported for B800 in refs 7 and 18 and whose parameters we attempted to utilize, exhibited atypically unstable behavior, which is far from the ensemble average probed by SHB. The reasons for the discrepancy can be understood if one recalls that, as estimated in ref 18, the small spectral shifts most likely originate from the interaction of the chromophore with the tunneling entities at the distance of approximately 1 nm away, which places these entities at the protein/amorphous host interface[55] and beyond. Although detergent-solubilized LH2 was used in the cases of both SHB and SPCS experiments, a 2:1 glycerol/water (buffer) mixture was employed in our experiments, whereas in low-temperature SPCS experiments, one would expect a poly(vinyl alcohol) (PVA) matrix with some amount of retained water. The difference in the sample preparation procedures could also explain the imperfect match between the sum of the many SPCS spectra and the bulk spectra. Because the light intensities employed in SPCS and SHB experiments are not very different and because the spectral diffusion behavior observed in SPCS experiments was intensity-independent, the possibility that the differences in the smallest-barrier tier dynamics can be attributed to a higher excitation intensity driving the molecules into conformational states that are less accessible or unavailable in the dark/lower-light conditions[28] is not very plausible, although it cannot be completely excluded.

On the other hand, one could argue that, in the SPCS experiments, the broader range of possible transition frequencies observed for single molecules on the lowest-barrier tier of the energy landscape is not a result of the higher excitation intensity, but is caused by the laser being scanned over a range of wavelengths and not kept at the same wavelength as in SHB experiments. In other words, in this scenario, the SPCS first cumulant distributions[18] adequately describe the whole range of conformations that can be assumed by the pigment−protein system, but the fixed excitation wavelength SHB cannot drive molecules far enough from their original transition frequencies. For HGK to be as slow as observed, one has to require that the single-step shifts of the molecule lines must be significantly smaller than the shifts of the single-molecule lines between two consecutive SPCS scans in ref 18. Only this would ensure that a molecule experiences multiple SHB events before leaving the resonance with the laser, thereby creating an illusion of very low SHB yield. This, in turn, means that the distributions of shifts of the single-molecule lines between the consecutive scans[18] must be a result of many, rather than one, very small shifts per SPCS scan, and our above estimates of λ_0 should be decreased further. The latter, however, would require a further reduction of the width of the antihole function, which would result in even poorer agreement between measured and simulated hole spectra than depicted in Figure 7B, and so on. One should also remember that, at some point of that iterative process, the mean of the tunneling parameter distribution λ_0 would be reduced to a level that made nonresonant burning with the white light of the FTIR spectrometer quite possible, and that would contradict the results of Figure 4. Namely, white-light-induced spectral shifts corresponding to this lowest-barrier tier of the energy landscape would cause the hole to broaden to the width of the first cumulant distribution from ref 18 while being filled. On the other hand, lack of broadening accompanied by noticeable hole filling in Figure 4 indicates that the white light of the FTIR spectrometer is already sufficient to cause or reverse conformational changes even on the next tier of the energy landscape.

To resolve these contradictions, one could argue that the lowest-barrier tier SHB yield is not small, but that the SPCS observations for this tier of the energy landscape have a transient character. That is, one could imagine the envelope of the lowest-barrier fraction of the landscape (see the dash-dotted line in the upper-right part of Figure 1) to be parabolic, with barriers between different substates being on the order of k_BT at 5 K. Then, a molecule that starts its path over the landscape from the deepest well and is pushed "up the funnel" by excitation, will "slide", with friction, back "down the funnel" on a time scale of seconds. In the case of SPCS, the molecule could be caught by the scanning laser at different stages of movement down the parabola, whereas in the case of SHB, the molecule

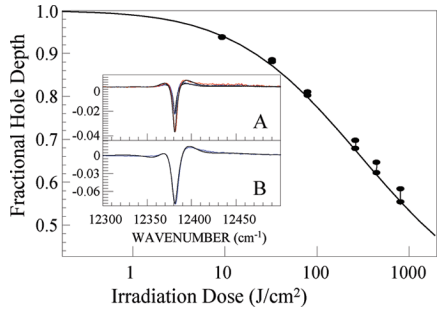

Figure 8. Main graph: Hole growth kinetics calculated with $\lambda_0 = 10.3$, $\sigma_\lambda = 0.8$, line width distribution from ref 4 and 5% probability of the largest ($\sim$60 cm^{-1}) shift, superimposed on experimental data. Inset A: Overall shape fit to the two shallowest holes in the series burned at 807.5 nm. Inset B: Overall shape fit to the deepest hole in the series. Noisy colored solid curves represent experimental data; smoother black curves are fits.

would get re-excited only after it reached the bottom/resonance with the laser. However, allowing for this mechanism is equivalent to allowing for transient holes, which contradicts our observation that the HGK curve (i.e., the dependence of the hole depth on irradiation dose while the laser is on) matches the data obtained from the spectral holes measured (minutes) after the burn has been stopped (i.e., with the burning laser off). To summarize, in our SHB experiments, we did not observe any evidence of spectral diffusion with parameters corresponding to the lowest-barrier tier of the protein energy landscape suggested by SPCS.

Thus, we had no choice but to proceed with the simultaneous gradual adjustment of the parameters of the tunneling distribution and of the antihole function in order to determine the set of numbers that would actually allow for a satisfactory match between our SHB data and simulations. The best fits to experimental data are presented in Figure 8. The main graph contains the fit to the HGK data, whereas the insets contain the fits (black lines) to holes obtained with low (A) and high (B) irradiation doses (colored lines). The simulation parameters are summarized in Table 1. The electron−phonon coupling parameters were fixed throughout the fitting procedure and correspond to the single complex spectra shapes from ref 23. Varying the Huang−Rhys factor S within reasonable limits does not affect the fits significantly. A slight increase of S can be compensated by a slight decrease of λ_0 (or vice versa) while preserving the quality of the fit. The line width distribution from ref 4 was also employed. Recall that Figure 6 shows the hole width dependence on fractional hole depth (diamonds) obtained with the same parameters as the data in Figure 8, along with the experimental data (triangles) and data simulated in the absence of the line width distribution but all other parameters being the same (circles). Obviously, the match is satisfactory when the distribution from ref 4 is employed. Concerning the use of the EET rate distribution based on the whole B850 DOS including upper excitonic components, it is unclear how the assumptions made to produce this distribution can be reconciled with the high-pressure SHB results,[34,41] which suggest independence of the B800 → B850 EET rates from the energies of the higher excitonic components of the B850 manifold. It would be extremely interesting to investigate whether, for example, the EET rate distributions for carotenoid-assisted B800 → B850 EET[56,57] would result in better agreement with the experimental data. (To the best of our knowledge, predictions concerning such distributions have not been developed so far.)

Several additional remarks can be made with respect to Table 1. First, the reported SHB yields for the medium (i.e., $\sim$10 cm^{-1}) and large (i.e., $\sim$60 cm^{-1}) shifts are in agreement with the photon budgets of the SPCS experiments; see subsection 4.3. In this work, all B800 molecules were assumed to be capable of $\sim$10 cm^{-1} spectral shifts, contrary to what was suggested based on the results of the SPCS experiments.[18] However, if one takes into account the parameters of the distribution of HB yields resulting from our analysis, there is no contradiction: Some molecules followed in SPCS experiments just did not experience the tier-2 shifts within the time frame of the SPCS experiment. Note that the 35 cm^{-1} fwhm of the antihole distribution on this tier of the energy landscape corresponds to the $\sim$9 cm^{-1} average shift regardless of direction; that is, it is in agreement with SCPS results. However, it is unclear whether the requirement for a "little nudge to the blue" (3 cm^{-1} blue shift of the antihole function) is an artifact resulting from the calculation algorithm used (e.g., insufficient number if iterations) or is a reflection of real physics, or both. One could argue that the spectral shifts toward global minimum on the protein energy landscape (corresponding to the maximum of the B800 band) could be slightly more probable than in the opposite direction. Rigorously testing this hypothesis through simulations requires the application of a wavelength-dependent shape for the antihole function, which is currently beyond our computing powers, and requires the introduction of additional free parameters to the model. The largest ($\sim$60 cm^{-1}) spectral shifts seem to be observed for only 5% of the B800 molecules (as assumed in calculating the spectra shown in inset B of Figure 8 and the HGK curve in the main graph of that figure). Closer examination of the low-dose hole spectra suggests that about 10% of molecules capable of larger shifts would be required to produce better fits to the lower-dose holes (see inset A in Figure 8, as well as the inset of Figure 2). Thus, it appears that, if a given molecule is capable of the tier-3 (60 cm^{-1} on average) shift at all, the average SHB yield of that process must be higher than that for tier-2. A small fraction of molecules capable of large shifts (tens of wavenumbers) suggests that the structural rearrangements responsible for tier-3 dynamics are atypical and are probably a consequence of some distortions of the normal structure of the LH2 complex. This suggestion, if confirmed, could also explain the dependence of the frequency of incidence of the large shifts on species[25] and sample preparation. Finally, in light of the results of Figure 4, which indicate a significant degree of spectral memory for tiers 2 and 3 of the energy landscape, we also attempted to fit the HGK data utilizing the perfect-memory model from ref 26, that is, the model where each pigment molecule is interacting with one and only one TLS. Satisfactory fits to HGK data (not shown for brevity) can be obtained for $\lambda_0 = 9.3$ with other fit parameters being the same as above. The latter simulation provides the lower limit of λ_0 for B800 band of LH2 because, according to the SPCS data,[18] more than two distinct states on the tier 2 of protein energy landscape were frequently observed. Interestingly, this lower limit for λ_0 is still significantly larger than typical λ_0 value obtained for various glasses.[13−15,26,37,38]

5. Conclusions

A modified SHB model was developed to account for the shape of the resonant holes (including antihole) allowing for multiple possible ZPL frequencies for every single molecule (no-spectral-memory model). In addition, the model includes effects of burn light polarization dependence, dispersion of the SHB yields resulting from dispersion of barrier parameters, and the distribution of homogeneous line widths. In general, the NPHB results reported herein are compatible with SPCS

results[7,10,16,18−25] and with protein models including several hierarchical tiers of the energy landscape,[11,12] except that the dynamics associated with the fastest (smallest-barrier) tier observed in SPCS experiments is not observed in SHB. In other words, our SHB results are incompatible with the behavior of the single B800 molecule lines observed and discussed in detail in refs 7, 18, and 25. Although the presence of fast small-barrier tier dynamics in our experiments cannot be entirely excluded, it is rather safe to suggest that the parameters of that dynamics (if present) would have to be significantly different from those obtained by SPCS. Thus, it is likely that the fastest-tier behavior observed in SPCS experiments is due to the dynamics of the amorphous host and/or of the protein/host interface[55] or is a reflection of host-induced and host-specific conformational changes in the protein. This suggestion has interesting implications for interpreting SPCS data for other systems, for instance Photosystem I, where an attempt was recently made to assign various low-energy antenna states to particular groups of chlorophylls based on the protein dynamics observed in SPCS experiments.[58,59] In light of the data discussed in this work, we suggest that not only the supposed looseness of the protein pocket, as proposed in refs 58 and 59, but also the closeness to the interface between the protein and the outside amorphous host environment, as well as the nature of the host matrix surrounding the protein complex, could affect the frequency and/or magnitude of the spectral shifts experienced by the single-molecule lines in photosynthetic complexes. The discrepancy concerning small-barrier tier behavior led us to conclude that, although SPCS experiments reveal an unprecedented level of detail concerning the behavior of individual complexes, it is still unclear whether they can provide, within a reasonable time, information on average or typical protein complex dynamics. Thus, we propose that measurements of hole/antihole structure and its evolution (during the hole burning process) should be more widely used in combination with SPCS and with the measurements of spectral diffusion in the dark (hole broadening). Data from such experiments (research in progress) could lead to the development of more accurate models of protein dynamics. This would also provide more quantitative statistical data on light-induced spectral diffusion in photosynthetic complexes. Finally, we note that the estimated distribution of B800 → B850 energy-transfer rates[4] (including the whole B850 density of states) is in reasonable agreement with the SHB modeling results, although it is possible that actual distribution could contain smaller contribution from the narrowest widths. However, it remains to be determined whether other B800 → B850 EET theories, better agreeing with high-pressure SHB data,[34,41] could also provide a good description of the hole shape evolution.

Abbreviations

Chl, chlorophyll; EET, excitation energy transfer; HGK, hole growth kinetics; λ, tunneling parameter; MLS, multilevel system; NPHB, nonphotochemical hole burning; PSB, phonon sideband; SDF, site distribution function; SHB, spectral hole burning; SPCS, single photosynthetic complex spectroscopy; SSA, single-site absorption; TLS, two-level system; ZPH, zero-phonon hole; ZPL, zero-phonon line.

Acknowledgment. This research was supported by NSERC, including a Discovery grant (V.Z. and N.H.) and an Undergraduate Summer Research Fellowship (D.G.). R.J. was supported by an NSF grant (CHE-0907958). The authors are thankful to Mike Reppert (KSU) for fruitful discussions.

References and Notes

(1) Hayes, J. M.; Small, G. J. *J. Phys. Chem.* **1986**, *90*, 4928.
(2) Gillie, J. K.; Small, G. J.; Golbeck, J. H. *J. Phys. Chem.* **1989**, *93*, 1620.
(3) Reinot, T.; Zazubovich, V.; Hayes, J. M.; Small, G. J. *J. Phys. Chem. B* **2001**, *105*, 5083.
(4) Jang, S.; Newton, M. D.; Silbey, R. J. *Phys. Rev. Lett.* **2004**, *92*, 218301.
(5) Scholes, G. D.; Fleming, G. R. *J. Phys. Chem. B* **2000**, *104*, 1854.
(6) Mukai, K.; Abe, S.; Sumi, H. *J. Phys. Chem. B* **1999**, *103*, 6096.
(7) Baier, J.; Richter, M. F.; Cogdell, R. J.; Oellerich, S.; Köhler, J. *J. Phys. Chem. B* **2007**, *111*, 1135.
(8) Riley, K. J.; Jankowiak, R.; Rätsep, M.; Small, G. J.; Zazubovich, V. *J. Phys. Chem. B* **2004**, *108*, 10346.
(9) Prokhorenko, V. I.; Holzwarth, A. R. *J. Phys. Chem. B* **2000**, *104*, 11563.
(10) Hofmann, C.; Aartsma, T. J.; Michel, H.; Köhler, J. *Proc. Natl. Acad. Sci. U.S.A.* **2003**, *100*, 15534.
(11) Frauenfelder, H.; Sligar, S. G.; Wolynes, P. G. *Science* **1991**, *254*, 1598.
(12) Fenimore, P. W.; Frauenfelder, H.; McMahon, B. H.; Young, R. D. *Physica A* **2005**, *351*, 1.
(13) Reinot, T.; Small, G. J. *J. Chem. Phys.* **2000**, *113*, 10207.
(14) Reinot, T.; Dang, N. C.; Small, G. J. *J. Lumin.* **2002**, *98*, 183.
(15) Reinot, T.; Small, G. J. *J. Chem. Phys.* **2001**, *114*, 9105.
(16) Berlin, Y.; Burin, A.; Friedrich, J.; Köhler, J. *Phys. Life Rev.* **2007**, *4*, 64.
(17) Berlin, Y.; Burin, A.; Friedrich, J.; Köhler, J. *Phys. Life Rev.* **2006**, *3*, 262.
(18) Baier, J.; Richter, M. F.; Cogdell, R. J.; Oellerich, S.; Köhler, J. *Phys. Rev. Lett.* **2008**, *100*, 018108.
(19) Hofmann, C.; Aartsma, T. J.; Michel, H.; Köhler, J. *New J. Phys.* **2004**, *6*, 8.
(20) van Oijen, A. M.; Ketelaars, M.; Köhler, J.; Aartsma, T. J.; Schmidt, J. *Biophys. J.* **2000**, *78*, 1570.
(21) Ketelaars, M.; van Oijen, A. M.; Matsushita, M.; Köhler, J.; Schmidt, J.; Aartsma, T. J. *Biophys. J.* **2001**, *80*, 1591.
(22) Matsushita, M.; Ketelaars, M.; van Oijen, A. M.; Köhler, J.; Aartsma, T. J.; Schmidt, J. *Biophys. J.* **2001**, *80*, 1604.
(23) Hofmann, C.; Michel, H.; van Heel, M.; Köhler, J. *Phys. Rev. Lett.* **2005**, *94*, 195501.
(24) Oikawa, H.; Fujiyoshi, S.; Dewa, T.; Nango, M.; Matsushita, M. *J. Am. Chem. Soc.* **2008**, *130*, 4580.
(25) Baier, J.; Gabrielsen, M.; Oellerich, S.; Michel, H.; van Heel, M.; Cogdell, R. J.; Köhler, J. *Biophys. J.* **2009**, *97*, 2604.
(26) Reinot, T.; Dang, N. C.; Small, G. J. *J. Chem. Phys.* **2003**, *119*, 10404.
(27) Janusonis, J.; Valkunas, L.; Rutkauskas, D.; van Grondelle, R. *Biophys. J.* **2008**, *94*, 1348.
(28) Rutkauskas, D.; Novoderezhkin, V. I.; Cogdell, R. J.; van Grondelle, R. *Biophys. J.* **2005**, *88*, 422.
(29) Rutkauskas, D.; Novoderezhkin, V. I.; Cogdell, R. J.; van Grondelle, R. *Biochemistry* **2004**, *43*, 4431.
(30) Novoderezhkin, V. I.; Rutkauskas, D.; van Grondelle, R. *Biophys. J.* **2006**, *90*, 2890.
(31) Reppert, M.; Zazubovich, V.; Dang, N. C.; Seibert, M.; Jankowiak, R. *J. Phys. Chem. B* **2008**, *112*, 9934.
(32) Neupane, B.; Dang, N. C.; Reppert, M.; Acharya, K.; Zazubovich, V.; Seibert, M.; Picorel, R.; Jankowiak, R. *J. Am. Chem. Soc.*, manuscript submitted
(33) Loll, B.; Kern, J.; Zouni, A.; Saenger, W.; Biesiadka, J.; Irrgang, K.-D. *Photosynth. Res.* **2005**, *86*, 175.
(34) Zazubovich, V.; Jankowiak, R.; Small, G. J. *J. Lumin.* **2002**, *98*, 123.
(35) Jankowiak, R.; Small, G. J. *Science* **1987**, *237*, 618.
(36) Kenney, M.; Jankowiak, R.; Small, G. J. *Chem. Phys.* **1990**, *146*, 47.
(37) Dang, N. C.; Reinot, T.; Reppert, M.; Jankowiak, R. *J. Phys. Chem. B* **2007**, *111*, 1582.
(38) Sigi, A.; Orrit, M.; Reinot, T.; Jankowiak, R.; Friedrich, J. *J. Chem. Phys.* **2007**, *127*, 084510.
(39) Wu, H.-M.; Rätsep, M.; Jankowiak, R.; Cogdell, R. J.; Small, G. J. *J. Phys. Chem. B* **1997**, *101*, 7641.
(40) Wu, H.-M.; Reddy, N. R. S.; Cogdell, R. J.; Muenke, C.; Michel, H.; Small, G. J. *Mol. Cryst. Liq. Cryst.* **1996**, *291*, 163.
(41) Zazubovich, V.; Jankowiak, R.; Small, G, J. *J. Phys. Chem.* **2002**, *106*, 6802.
(42) Wu, H.-M.; Savikhin, S.; Reddy, N. R. S.; Jankowiak, R.; Cogdell, R. J.; Struve, W. S.; Small, G. J. *J. Phys. Chem.* **1996**, *100*, 12022.
(43) Zazubovich, V.; Tibe, I.; Small, G. J. *J. Phys. Chem. B* **2001**, *105*, 12410.
(44) Bogner, U.; Schwarz, R. *Phys. Rev. B* **1981**, *24*, 2846.

(45) Shu, L.; Small, G. J. *J. Opt. Soc. Am. B* **1992**, *9*, 724.
(46) Kolaczkowski, S. V.; Hayes, J. M.; Small, G. J. *J. Phys. Chem.* **1994**, *98*, 13418.
(47) Pullerits, T.; Hess, S.; Herek, J. L.; Sundström, V. *J. Phys. Chem. B* **1997**, *101*, 10560.
(48) Wendling, M.; van Mourik, F.; van Stokkum, I. H. M.; Salverda, J. M.; Michel, H.; van Grondelle, R. *Biophys. J.* **2003**, *84*, 440.
(49) Alden, R. G.; Johnson, E.; Nagarajan, V.; Parson, W. W.; Law, C. J.; Cogdell, R. G. *J. Phys. Chem. B* **1997**, *101*, 4667.
(50) Rätsep, M.; Pajusalu, M.; Freiberg, A. *Chem. Phys. Lett.* **2009**, *479*, 140.
(51) Pieper, J.; Rätsep, M.; Irrgang, K.-D.; Freiberg, A. *J. Phys. Chem. B* **2009**, *113*, 10870.
(52) Rätsep, M.; Pieper, J.; Irrgang, K.-D.; Freiberg, A. *J. Phys. Chem. B* **2008**, *112*, 110.
(53) Freiberg, A.; Rätsep, M.; Timpmann, K.; Trinkunas, G.; Woodbury, N. W. *J. Phys. Chem. B* **2003**, *107*, 11510.
(54) Freiberg, A.; Rätsep, M.; Timpmann, K.; Trinkunas, G. *J. Lumin.* **2004**, *108*, 107.
(55) Heuer, A.; Neu, P. *J. Chem. Phys.* **1997**, *107*, 8686.
(56) Krueger, B. P.; Scholes, G. D.; Gould, I. R.; Fleming, G. R. *Phys. Chem. Comm.* **1999**, 8.
(57) Hu, X.; Damjanovic, A.; Ritz, T.; Schulten, K. *Proc. Natl. Acad. Sci. U.S.A.* **1998**, *95*, 5935.
(58) Brecht, M.; Studier, H.; Elli, A. F.; Jelezko, F.; Bittl, R. *Biochemistry* **2007**, *46*, 799.
(59) Brecht, M.; Radics, V.; Nieder, J. B.; Studier, H.; Bittl, R. *Biochemistry* **2008**, *47*, 5536.

JP9089358